Metals **2012**, *2*, 113-121; doi:10.3390/met2020113

OPEN ACCESS

metals

ISSN 2075-4701

www.mdpi.com/journal/metals/

Article

Thermal Conductivity Computations of Sintered Hollow Sphere Structures

Christoph Veyhl [1,*], Thomas Fiedler [1], Tobias Herzig [2], Andreas Öchsner [1,3], Timo Bernthaler [2], Irina V. Belova [1] and Graeme E. Murch [1]

[1] Centre for Mass and Thermal Transport in Engineering Materials, School of Engineering, The University of Newcastle, Callaghan, NSW 2308, Australia; E-Mails: thomas.fiedler@newcastle.edu.au (T.F.); irina.belova@newcastle.edu.au (I.V.B.); graeme.murch@newcastle.edu.au (G.E.M.)

[2] Department of Surface Engineering and Materials Science, Faculty of Mechanical and Materials Engineering, University of Applied Sciences Aalen, Aalen 73430, Germany; E-Mails: tobias.herzig@web.de (T.H.); timo.bernthaler@htw-aalen.de (T.B.)

[3] Department of Solid Mechanics and Design, Faculty of Mechanical Engineering, Technical University of Malaysia, UTM Skudai, Johor 81310, Malaysia; E-Mail: andreas.oechsner@gmail.com

* Author to whom correspondence should be addressed; E-Mail: christoph.veyhl@uon.edu.au; Tel.: +61-249-216-804; Fax: +61-249-216-946.

Received: 17 April 2012; in revised form: 10 May 2012 / Accepted: 14 May 2012 / Published: 30 May 2012

Abstract: The thermal conductivity of sintered hollow sphere structures (HSS) is investigated within the scope of this paper. For this purpose, finite element analyses based on micro-computed tomography images are performed on HSS structures. The complex geometry of the real sintered HSS sample is accurately captured with this new hybrid method. The numerical computations are investigated in three perpendicular directions (*i.e.*, *x*, *y* and *z*) in order to examine the anisotropic material behaviour. The results indicate that sintered HSS reveals quasi-isotropic behaviour in terms of effective thermal conductivity. For the first time, the influence of the sphere wall thickness of real HSS is investigated. To this end, the computed tomography data is carefully manipulated by changing the thickness of the hollow sphere wall. The variation of the wall thickness alters the relative density and has a significant influence on the thermal conductivity. The influence of the relative density on the thermal conductivity reveals a linear dependency.

Keywords: hollow sphere structure; cellular material; micro-computed tomography; finite element analysis; thermal conductivity

1. Introduction

Cellular materials are frequently represented in nature e.g., wood, cork, coral, trabecular bone [1,2], *etc*. Due to their superior specific properties such as lightweight, energy absorption, damping behaviour, large surface area, sound absorption and low thermal conductivity compared to the properties of the solid material [3,4], cellular structures are mimicked in industrial applications. Cellular materials can be distinguished by cell topology (*i.e.*, open-cell-, closed-cell, regular cell- and irregular cell-structure), morphology (*i.e.*, cell size, cell shape and cell orientation) and relative density (*i.e.*, ratio between solid volume fraction of the cellular material divided by the volume of the cellular material) [3].

Recently a new type of cellular material made of hollow spheres become available. Hollow spheres are commercially manufactured by the company hollomet GmbH, Dresden, Germany. The manufacturing process was developed by Fraunhofer Institute IFAM, Dresden, Germany [4–6] in collaboration with hollomet GmbH. At the beginning, organic spheres (*i.e.*, Styrofoam™ spheres) are coated with metal powder-binder suspension in a turbulence device. The produced green bodies can either be sintered as single spheres or sintered in bulk in order to form an interdependent structure with randomly distributed hollow spheres. In this study, sintered hollow sphere structure (HSS) with randomly distributed hollow spheres is considered. In the case of single spheres, an ordered structure can be generated with the help of a robot and the so-called "High Precision Pick and Place System" [7]. Alternatively, the single spheres can be used in randomly distributed structures and different joining technologies can be applied such as soldering, adhering and sintering. The adhering process allows the usage of two different methods, namely syntactic HSS where hollow spheres are embedded in a matrix (*i.e.*, epoxy resin or metal) or partial HSS (similar to sintered structures) where the hollow spheres are only glued in proximity to contact points [4].

In general, the hollow sphere structure can be influenced by following parameters: base material of the sphere wall, sphere diameter (*i.e.*, 0.5 mm–10 mm) [5], cell wall thickness (*i.e.*, 20 μm–1,000 μm) [5], micro-porosities in the sphere wall due to the sintering process [5], carbon content in the sphere wall caused by incineration of the Styrofoam™ sphere templates [8], structure (*i.e.*, ordered or randomly distributed), joining technology (*i.e.*, sintered, soldered, syntactically or partially adhered).

The sintered HSS is characterised by its homogeneous material behaviour due to less variation of pore geometries (*i.e.*, sphere shape, sphere wall thickness and sphere size). In contrast, closed-cell foam such as Alporas® or open-cell sponge m-pore® represent heterogeneous material properties in consequence of the different pore sizes, pore shapes and pore orientations [4,9].

Hollow sphere structures are multifunctional materials which possess interesting mechanical, thermal and acoustical properties [10]. Interesting industrial applications often make use of this multi-functionality, *i.e.*, a thermal insulator that simultaneously acts as a structural component [11]. The current paper is focused on the thermal properties of sintered HSS. Different approaches can be used in order to determine the thermal conductivity: experiments, analytical models and numerical

methods. The transient plane source (TPS) method is an experimental method for the determination of the thermal conductivity. Thermal conductivity of sintered HSS with randomly distributed spheres, partial HSS and syntactic HSS were investigated with the TPS method [12,13]. Another approach to characterise the thermal conductivity is analytical modelling. Solorzano [12] used the scaling law in order to describe random sphere arrangements of sintered HSS. Fiedler [13] used the Misnar model to describe the thermal conductivity of primitive cubic arrangement of partial and syntactic HSS. Another possibility for the thermal conductivity determination is the numerical computation. These calculations can be performed with the Finite Element Method (FEM) or Lattice Monte Carlo method (LMC). The model for the calculation can either be simplified [13,14] or based on real geometry [15–18] with the help of micro-computed tomography images. Fiedler *et al.* [19,20] investigated the influence of the HSS wall thickness of simplified primitive cubic models. Two different hollow sphere structures were investigated namely partial HSS and syntactic HSS. Vesenjak *et al.* [21,22] investigated the heat transfer in closed-cell cellular material and honeycomb structure with different gaseous pore filler and performed transient computational simulations.

This study takes the research an important step further. The real geometry of sintered hollow sphere material is analysed and different models with varying sphere wall thicknesses are considered. In addition, the study considers the micro-porosity of the sphere wall that is introduced by the sintering process. This is accomplished with the usage of a Maxwell–type expression.

2. Methodology and Material

2.1. Numerical Modeling

Numerical modelling consists of the following steps: micro-computed tomography data acquisition, generation of a three-dimensional model, triangulated surface mesh generation, volume mesh generation and FE-analysis. A detailed description of this process is given in [23].

Figure 1. 3D-object of the micro-computed tomography record with applied boundary conditions.

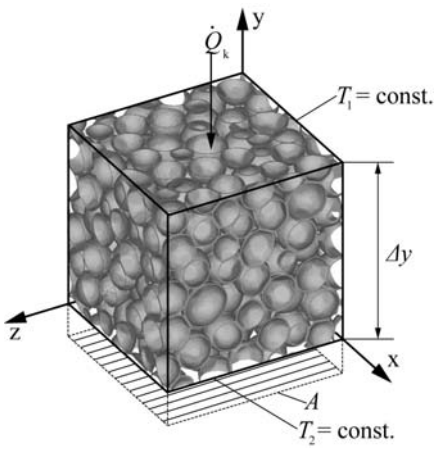

Figure 1 shows the boundary conditions of the finite element model for thermal conductivity calculations in *y*-direction. The thermal conductivity can be determined in three perpendicular directions (*i.e.*, *x*, *y* and *z*) by changing the constant temperature planes. All calculations are performed

under steady state conditions and the four lateral surfaces are adiabatic where no thermal energy exchange occurs with the surrounding. The nodal heat reaction flux $\dot{Q}_k$ perpendicular to the surfaces with the constant temperature is calculated by the finite element analysis. The total heat flux $\dot{Q}$ is the sum of the single nodal heat fluxes $\dot{Q}_k$ through one of the boundary surfaces. Within this study, the thermal radiation effect on heat transfer is neglected since its contribution is very low for the relevant temperature range which is below 700 K [24]. The influence of thermal convection is also disregarded because sintered HSS represents mainly a closed-cell structure with a low volume fraction of interconnected porosity [2]. In this study, pores are assumed to be filled with air. Due to the low thermal conductivity of the gas mixture, conductive heat transfer inside the pore space is negligible. These assumptions simplify the mathematical description of the heat transfer and the effective thermal conductivity can be calculated according to Equation (1) with Fourier's law.

$$\lambda_{\text{eff}} = \frac{\dot{Q} \cdot \Delta y}{A \cdot (T_2 - T_1)} \tag{1}$$

The parameters of Fourier's law are given in this paragraph: $\dot{\boldsymbol{Q}}$ = heat flux, Δy = spatial distance between two opposing boundary surfaces, A = projected area, T_1 = temperature on the top, T_2 = temperature on the bottom. The geometry shown in Figure 1 consists of approximately 5 cells per edge length and consequently possesses about 5^3 = 125 cells in total. This number exceeds the approximately 100 cells required for a representative volume [15]. The model size is 18 × 18 × 18 mm and is represented by 400^3 voxels resulting in a resolution of 0.045 mm/voxel. The FE-model consists of roughly five million elements (*i.e.*, hexahedral-, tetrahedral- and pentahedral elements).

2.2. Material

Every sinterable material can be used in order to manufacture HSS with the powder based processing technique. Some thermal conductivities are given in the following text where the thermal conductivity is shown in brackets: titanium (6.9 W/m K), stainless steel (12.8 W/m K), high carbon steel (50 W/m K), pure molybdenum (138 W/m K) and aluminium (180 W/m K) [12]. Micro pores appear in the sphere wall due to the powder based manufacturing method and decrease thermal conductivity. Optical microscopy images are analysed of sintered HSS made of high carbon steel and a micro-porosity of p = 3.8% was detected. Based on this value, a correction factor C_1 is calculated with the Maxwell-type expression [15,25] in order to account for the decrease in conductivity due to micro-porosity. This model assumes that all micro-pores are of similar size and homogeneously distributed in the sphere wall.

$$C_1 = \frac{2 \cdot (1 - p)}{2 + p} = 0.944 \tag{2}$$

The second influence on the effective thermal conductivity is the meso-structure which is denoted as C_2. Finally, the effective thermal conductivity can be calculated with Equation (3), which incorporates the thermal conductivity λ_B of the base material, the micro-porosity C_1 and meso-structure C_2.

$$\lambda_{\text{eff}} = C_1 \cdot C_2 \cdot \lambda_B \tag{3}$$

3. Numerical Results

3.1. Convergence Analysis

The convergence analysis for the sintered HSS is performed on a smaller fraction of the calculation model (*i.e.*, side length 7.5 mm) in order to reduce calculation time. The convergence analysis can be distinguished between geometrical convergence and numerical convergence. The geometric convergence requires a sufficient number of elements in order to accurately capture the complex geometry by using primitive geometric element shapes (*i.e.*, tetrahedrons, pentahedrons and hexahedrons). Numerical convergence is achieved by an adequate number of nodes for the mathematical description of the temperature field. The results of the convergence analysis are shown in Table 1 along with the mesh density, which is the number of elements divided by the solid volume fraction of the model. The absolute volume deviation $|\Delta V|$ is used to quantify geometric convergence shown in Equation (4).

$$|\Delta V| = |V_{3D} - V_{FE}| / V_{3D} \tag{4}$$

Variable V_{3D} is the solid volume of the micro-computed tomography data set and V_{FE} is the solid volume of the discretised calculation model. For perfect geometry the accuracy of the absolute volume deviation $|\Delta V|$ becomes zero. Numerical convergence is ensured for models with mesh densities of 0.88 or higher, *i.e.*, the conductivity does not significantly change. Accordingly, the mesh density of 0.88 is chosen for all following computational models.

Table 1. Convergence analysis of the sintered hollow sphere structure (HSS) models.

Elements	**Nodes**	**Mesh density**	V_{3D}	V_{FE}	$\|\Delta V\|$	λ
[−]	[−]	[Elements/V_{voxels}]	[−]	[−]	[−]	[%]
212941	90151	0.30	0.149	0.15	0.00671	9.15
343344	154412	0.49	0.149	0.15	0.00671	9.14
622385	311255	0.88	0.149	0.149	0	9.05
1489933	790252	2.13	0.149	0.149	0	9.05
2509508	1424344	3.57	0.149	0.149	0	9.03
5114321	3136257	7.14	0.149	0.149	0	9.03

3.2. Results and Discussion

Figure 2 shows the five investigated geometries. All models exhibit different relative densities or wall thickness to radius ratios t_w/r. The radius and wall thickness are averaged measurement values based on evaluated computed tomography cross sectional images. Figure 2a shows the original geometry obtained by μCT images of a real HSS sample and Figure 2e the modified geometry with completely filled spheres. The intermediate modifications to the sphere wall thickness are shown in Figure 2(b–d) where the sphere wall thickness is progressively increased towards the inside of the spheres. This task was carried out by altering the wall thickness on each recorded micro-computed tomography image. Note, that the volume deviation (*i.e.*, Equation (4)) between the 3D-object and the discretised finite element model is less than 0.7% for all models. This means that, the geometry is captured very well with the discretised numerical models. The difference between the thermal

conductivities in three perpendicular directions (*i.e.*, *x*, *y* and *z*) and their arithmetical mean is less than 2% in all cases. Therefore, the sintered HSS exhibit quasi-isotropic material behaviour in terms of the thermal conductivity. In contrast, other cellular materials such as m-pore® and Alporas® reveal anisotropic material behaviour [18]. Figure 4a shows the arithmetical mean (*i.e.*, *x*, *y* and *z*) of the normalised thermal conductivity plotted as a function of the relative density ρ_r. It can be seen that the numerical data points follow very well a linear regression line. This is also shown with the coefficient of determination $R^2 = 0.99$ [9]. In addition, the results are in good agreement with a linear function by Fiedler *et al.* [16] formulated to predict the normalised conductivity for thin-walled structures. Finally, good agreement is obtained with a previous thermal analysis of sintered HSS based on micro-computed tomography [15] (see triangular marker in Figure 4a). Figure 4b shows the arithmetical mean (*i.e.*, *x*, *y* and *z*) of the normalised thermal conductivity as a function of the ratio of wall thickness t_w to radius *r*. Numerical results are shown by filled squares and can be described very well with a 2nd order polynomial regression. The good agreement between numerical data points and polynomial regression is shown with the R^2 value of 0.99.

Figure 2. Evolution of sintered HSS models. (**a**) $t_w/r = 0.066$, $\rho_r = 0.15$; (**b**) $t_w/r = 0.18$, $\rho_r = 0.32$; (**c**) $t_w/r = 0.31$, $\rho_r = 0.46$; (**d**) $t_w/r = 0.53$, $\rho_r = 0.63$; (**e**) $t_w/r = 1.0$ $\rho_r = 0.744$.

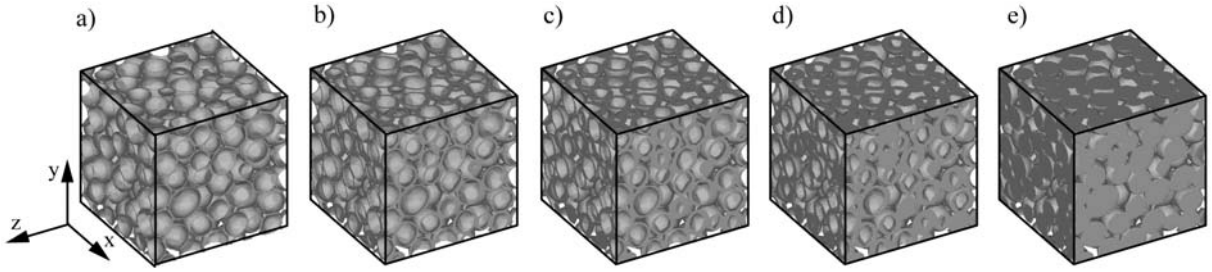

It must be mentioned that the packing density ϕ (*i.e.*, the fraction of the volume occupied by the filled spheres) is $\phi = 0.744$. It is interesting to compare this value with the maximum possible packing density $\phi_{max} \approx 0.74$ of spherical particles and typical packing densities of spherical packed beds $\phi = 0.64$ [26]. The high value $\phi = 0.744$ of the investigated geometry is slightly more than the theoretical maximum which can be explained by plastic deformation during the manufacturing process. The spheres are flattened on the diffusion bonded contact area (see Figure 3) between the hollow spheres resulting in good thermal contact of neighbouring spheres (as opposed to point contact). The current study aims to model the change of conductivity with increasing radius ratio t_w/r. However, the manufacturing of sintered HSS with thicker sphere walls is likely to yield less plastic deformation due to the rapidly increasing strength of the spheres. This results in smaller contact areas between neighbouring spheres. As a consequence, the numerical results of the current study are strictly valid for the considered model structures but may slightly overestimate the conductivities of real structures.

Figure 3. Optical microscopy image of the diffusion bonded contact between two adjacent hollow spheres.

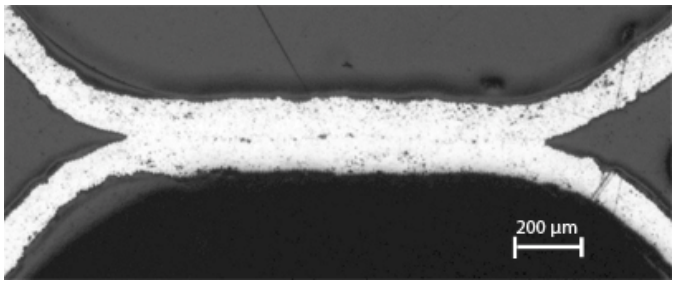

Figure 4. (**a**) Normalised thermal conductivity vs. relative density; (**b**) Normalised thermal conductivity vs. ratio wall thickness to radius.

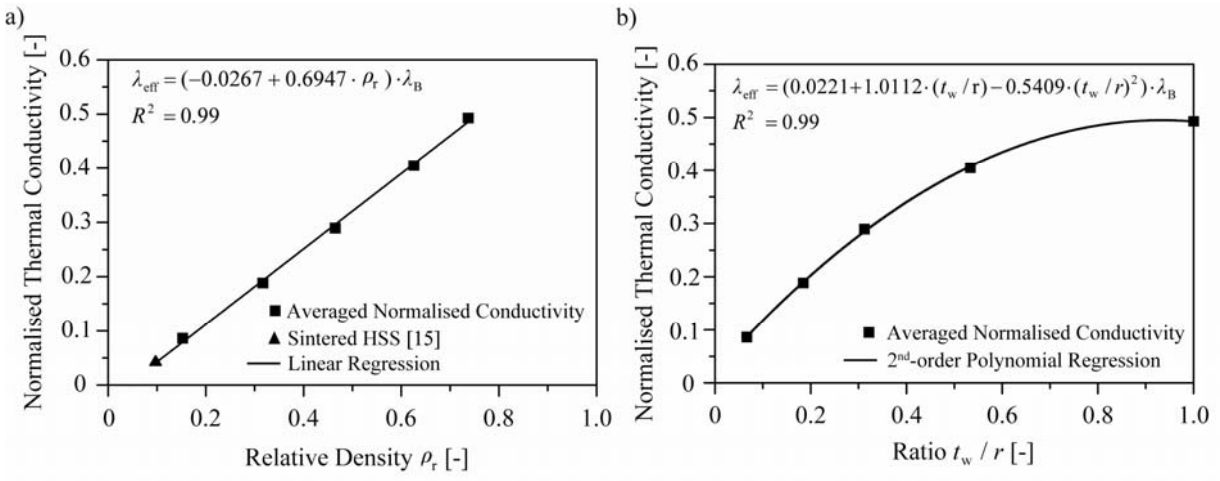

4. Conclusions

In this paper, the averaged normalised thermal conductivity of sintered HSS has been investigated. Calculations were performed with the finite element method based on micro-computed tomography images. Sphere wall thickness was modified in order to obtain different relative densities and wall thickness to radius ratios. Quasi-isotropic material behaviour is observed with less than 2% deviation of directional conductivities and this is in agreement with results by Fiedler *et al.* [15]. Based on the finite element results, the change of the thermal conductivity with respect to the relative density can be accurately described with a linear regression line. Alternatively, a 2nd order polynomial regression can be used to model the functional dependence of the normalised thermal conductivity on the sphere wall to radius ratio t_w/r.

Acknowledgments

Research support from the Australian Research Council is gratefully acknowledged. Christoph Veyhl gratefully acknowledges the University of Newcastle, Centre for Mass and Thermal Transport in Engineering Materials for its funding support. The authors would like to thank the hollomet GmbH, Dresden, Germany for supporting the work with providing hollow sphere samples.

References

1 Gibson, L.J.; Ashby, M.F.; Harley, A.B. *Cellular Materials in Nature and Medicine*; Cambridge University Press: New York, NY, USA, 2010.

2 Gibson, L.J.; Ashby, M.F. *Cellular Solids-Structure and Properties*, 2nd ed; Cambridge University Press: New York, NY, USA, 2001.

3 Ashby, M.F.; Evans, A.; Fleck, N.A.; Gibson, L.J.; Hutchinson, J.W.; Wadley, H.N.G. *Metal Foams: A Design Guide*; Butterworth-Heinemann: Oxford, UK, 2000.

4 Fiedler, T. *Numerical and Experimental Investigation of Hollow Sphere Structures in Sandwich Panels*; Trans Tech Publications: Stafa, Zurich, 2008.

5 Stephani, G.; Quadbeck, P.; Andersen, O. New multifunctional lightweight materials based on cellular metals-manufacturing, properties and applications. In *Proceedings of the International Conference on Advanced Structural and Functional Materials Design*, Osaka, Japan, 10–12 November 2008.

6 Banhart, J. Manufacture, characterisation and application of cellular metals and metal foams. *Prog. Mater. Sci.* **2001**, 46, 559−632.

7 Lösch Cellular Engineering Ziviltechniker GesmbH Home Page. Avaliable online: http://lce.co.at (accessed on 15 May 2012).

8 Studnitzky, T.; Andersen, O. Control of the carbon content in metal hollow sphere structures by variation of the debindering condtions. In *Proceedings of the Symposium on Cellular Metals and Polymers*, Fürth, Germany, 12–14 October 2004.

9 Veyhl, C.; Belova, I.V.; Murch, G.E.; Fiedler, T. Finite element analysis of the mechanical properties of cellular aluminium based on micro-computed tomography. *Mater. Sci. Eng. A* **2011**, *528*, 4550–4555.

10 Öchsner, A.; Augustin, C. *Multifunctional Metallic Hollow Sphere Structures*; Springer: Berlin, Germany, 2009.

11 Evans, A.G.; Hutchinson, J.W.; Ashby, M.F. Cellular metals. *Curr. Opin. Solid State Mater. Sci.* **1998**, *3*, 288–303.

12 Solórzano, E.; Rodríguez-Perez, M.A.; de Saja, J.A. Thermal conductivity of metallic hollow sphere structures: An experimental, analytical and comparative study. *Mater. Lett.* **2009**, *63*, 1128–1130.

13 Fiedler, T.; Solórzano, E.; Öchsner, A. Numerical and experimental analysis of the thermal conductivity of metallic hollow sphere structures. *Mater. Lett.* **2008**, *62*, 1204–1207.

14 Öchsner, A.; Tane, M.; Nakajima, H. Prediction of the thermal properties of lotus-type and quasi-isotropic porous metals: Numerical and analytical methods. *Mater. Lett.* **2006**, *60*, 2690–2694.

15 Fiedler, T.; Löffler, R.; Bernthaler, T.; Winkler, R.; Belova, I.V.; Murch, G.E.; Öchsner, A. Numerical analyses of the thermal conductivity of random hollow sphere structures. *Mater. Lett.* **2009**, *63*, 1125–1127.

16 Fiedler, T.; Belova, I.V.; Murch, G.E. Theoretical and Lattice Monte Carlo analyses on thermal conduction in cellular metals. *Comput. Mater. Sci.* **2010**, *50*, 503–509.

17 Fiedler, T.; Solórzano, E.; Garcia-Moreno, F.; Öchsner, A.; Belova, I.V.; Murch, G.E. Computed tomography based finite element analysis of the thermal properties of cellular aluminium. *Mater. Sci. Eng. Technol.* **2009**, *40*, 139–143.
18 Veyhl, C.; Belova, I.V.; Murch, G.E.; Öchsner, A.; Fiedler, T. Thermal analysis of aluminium foam based on micro-computed tomography. *Mater. Sci. Eng. Technol.* **2011**, *42*, 350–355.
19 Fiedler, T.; Öchsner, A. Influence of the morphology of joining on the heat transfer properties of periodic metal hollow sphere structures. *Mater. Sci. Forum* **2007**, *553*, 45–50.
20 Fiedler, T.; Öchsner, A. On the thermal conductivity of adhesivley bonded and sintered hollow sphere structures (HSS). *Mater. Sci. Forum* **2007**, *553*, 39–44.
21 Vesenjak, M.; Žunič, Z.; Öchsner, A.; Hribersek, M.; Ren, Z. Heat conduction in closed-cell cellular metals. *Mater. Sci. Eng. Technol.* **2005**, *36*, 608–612.
22 Vesenjak, M.; Žunič, Z.; Ren, Z.; Öchsner, A. Computational study of heat transfer in honeycomb structures accounting for gaseous pore filler. *Defect Diffus. Forum* **2008**, *273–276*, 699–706.
23 Veyhl, C.; Belova, I.V.; Murch, G.E.; Öchsner, A.; Fiedler, T. On the mesh dependence of non-linear mechanical finite element analysis. *Finite Elem. Anal. Des.* **2010**, *46*, 371–378.
24 Lu, T.J.; Chen, C. Thermal transport and fire retardance properties of cellular aluminium alloys. *Acta Mater.* **1999**, *47*, 1469–1485.
25 Maxwell, J.C. *A Treatise on Electricity and Magnetism*; Clarendon Press: Calfornia, CA, USA, 1892.
26 Jaeger, H.M.; Nagel, S.R. Physics of granular state. *Science* **1992**, *255*, 1523–1531.